

# Characteristic Analysis of an Traveling Wave Ultrasonic Motor using a Cylindrical Dynamic Contact Model

Jong-Suk Ro<sup>†</sup>, Kyung-Pyo Yi\*, Tae-Kyung Chung\*\* and Hyun-Kyo Jung\*

**Abstract** – The traveling wave ultra-sonic motor (TWUSM) is operated through the frictional force between the rotor and the stator. Hence, the contact mechanism should be analyzed to estimate the motor performance. However, the nonlinearity of the contact mechanism of the TWUSM makes it difficult to propose a proper contact model and a characteristic analysis method. To address these problems, a novel contact model is proposed and be termed the cylindrical dynamic contact model (CDCM) in this research. An estimation method of the motor performance is proposed using the CDCM, an analytical method, and a numerical method. The feasibility and usefulness of the proposed characteristic analysis are verified through experimental data.

**Keywords:** Actuator, Contact, Energy conversion, Finite element method, Nonlinear, Traveling wave, Ultrasonic motor.

## 1. Introduction

The nonlinearity of the contact mechanism of the TWUSM has been made it difficult to propose an effective characteristic analysis method [1-6]. Hence, many researchers have investigated the contact mechanisms of TWUSMs over the past few decades. Numerous types of characteristic analysis methods using diverse kinds of contact models have been proposed for the TWUSM by many researchers [2, 7-13]. However, some of the proposed methods have to use the unreasonable values of material coefficients or inconsistent material coefficients to fit the calculated data to the simulated results. In some methods, the governing equations are complex to be solved. Some methods can analyze the partial characteristics of the motor performance. To address these conventional problems, a novel contact model for the TWUSM, which referred to CDCM, is proposed in this research. Furthermore, a characteristic analysis method using the proposed CDCM, an analytical method, and a numerical method for the TWUSM is proposed in this paper. The proposed method for the TWUSM is verified by experimental data with a prototype of the TWUSM.

## 2. Working Principle of the TWUSM

Fig. 1 illustrates the working principle of the TWUSM.

For the generation of the traveling wave, the piezoelectric materials are placed in the stator with a proper space difference. By applying electrical power to the piezoelectric materials with a proper time difference, the travelling wave is generated at the stator. As shown in Fig.1, by contacting the rotor to the stator and applying mechanical pressure, the rotor moves by the frictional force between the rotor and the stator.

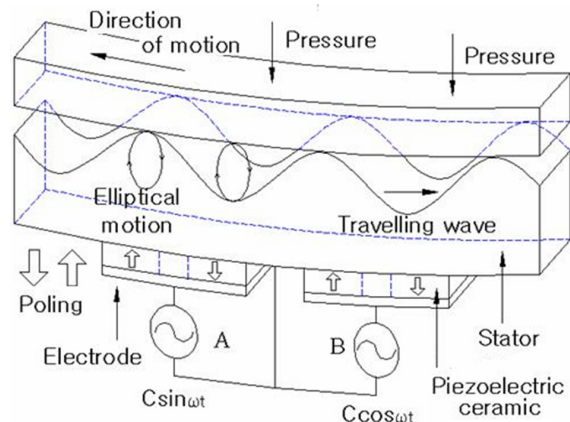


Fig. 1. Working principle of the TWUSM.

## 3. Characteristic Analysis Method using the CDCM

### 3.1 CDCM

As shown in Fig. 2, we assumed the stator and the rotor of the TWUSM as cylindrical bodies with the radius of  $R_1$  and  $R_2$ , respectively. To reflect the dynamic contact condition, the CDCM is proposed as illustrated in Fig. 3,

<sup>†</sup> Corresponding Author: Korea Electrical Engineering & Science Research Institute, Seoul, Korea. (jongsukro@naver.com)

\* Dept. of Electrical and Computer Engineering, Seoul National University, Korea. (ruinedsky@elecmech.snu.ac.kr, hkjung@snu.ac.kr)

\*\* Dept. of Electrical and Electronics Engineering, Chung-Ang University, Korea. (tkchung@cau.ac.kr)

Received: January 30, 2013; Accepted: June 5, 2013

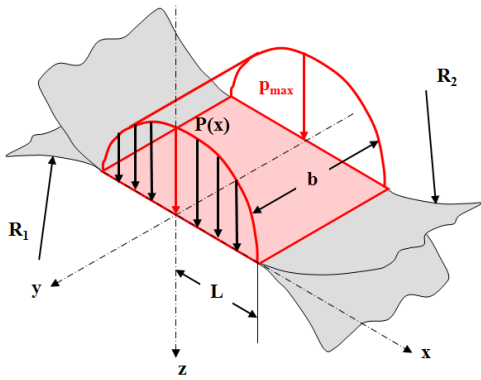


**Fig. 2.** Modeling of a rotor and a stator using cylinders.

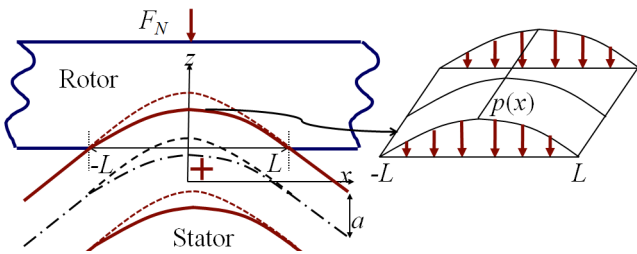


**Fig. 3.** The proposed CDCM for the TWUSM.

describing the nonlinear deformation at the area of contact. It is assumed that both rolling and sliding occur between the stator and the rotor while they are in contact.

### 3.2 Analysis of TWUSM using the FEM

The first step for the characteristic analysis of the TWUSM is the calculation of the operating frequency  $f$  (Hz) and the displacement amplitude  $A$  (m) of the TWUSM by means of 3D-FEM. We developed the 3D-FEM software and an auto-mode search program. The operating frequency can be calculated through an impedance analysis using FEM and (1), in which  $Z(\omega)$  is the impedance at the excitation frequency  $\omega$  (rad/sec),  $\Phi(\omega)$  (V) is the electric potential on the electrode, and  $Q_0$  (C) is the electric charge.

$$Z(\omega) = \frac{\Phi(\omega)}{j\omega Q_0} \quad (1)$$

### 3.3 Formula for the motion of a stator

Based on Kirchhoff's plate theory, the neutral plane of the stator can be expressed in terms of an ideal traveling wave as (2) while assuming that the stator is not affected by the contact force [1-3, 11]. Here,  $r$  is the position in the radial direction,  $R(r)$  is the amplitude at radius  $r$ ; and  $n$  is the number of nodal lines.

$$w(r, \phi, t) = R(r) \cos(n\phi - \omega t) \quad (2)$$

The three-dimensional problem can be replaced by a two-dimensional problem, as expressed by (3).

$$w(\hat{x}, t) = A \cos\left(\frac{2\pi\hat{x}}{\lambda} - \omega t\right) \quad (3)$$

which is subject to

$$\lambda = \frac{l_{eff}}{n} \quad (4)$$

$$l_{eff} = 2\pi r_{eff} \quad (5)$$

$$r_{eff} = \frac{d_{out} + d_{in}}{4} \quad (6)$$

where  $A$  is the normal displacement amplitude of the neutral plane for a stator,  $\lambda$  is the wavelength,  $l_{eff}$  (m) is the effective length of the circumference of the contact area,  $r_{eff}$  (m) is the effective radius of the contact area, and  $d_{out}$  (m) and  $d_{in}$  (m) are respectively the outer and the inner diameter of the contact area. The contact problem is described in a fixed reference  $(\hat{x}, \hat{z})$  in (3). This can be transformed to a moving reference  $(x, z)$  using (7) and (8), where  $v_w$  is the wave propagation velocity (m/sec).

$$\hat{x} = x + v_w t \quad (7)$$

$$v_w = \frac{\lambda \omega}{2\pi} \quad (8)$$

The moving reference follows the wave crest. Hence, (3) can be formulated into the time-independent Eq. (9) by substituting (7) and (8) into (3). The normal displacement of the neutral plane of the stator in the moving reference can be derived as (10).

$$w(\hat{x}, t) = w(x + v_w t, t) = A \cos\left(\frac{2\pi}{\lambda}(x + v_w t) - \omega t\right) \quad (9)$$

$$w(x, t) = A \cos\left(\frac{2\pi x}{\lambda}\right) \quad (10)$$

### 3.4 Analysis of the contact length

When two cylinders, which are the stator and the rotor, come into contact with each other, as shown in Fig. 2, the half of the contact length  $L$  can be calculated by (11), where  $m_1$  and  $m_2$  are the material coefficients of the stator and the rotor, respectively;  $B$  is the shape coefficient of the cylinder;  $F_{N-unit}$  (N/m) is the normal force per unit length in the radial direction at the unit wave;  $E_1$  (Pa) and  $E_2$  (Pa) are the equivalent elasticity modulus for the stator and the rotor, respectively;  $\nu_1$  and  $\nu_2$  are the Poisson's ratios of the stator and the rotor, respectively;  $F_N$  (N) is the normal force applied to the TWUSM for the frictional force; and  $b$  is the contact width in the radial direction.

$$L = \sqrt{\frac{2}{\pi} \frac{m_1 + m_2}{B} F_{N\text{-unit}}} \quad (11)$$

which is subject to

$$m_1 = \frac{1 - v_1^2}{E_1} \quad (12)$$

$$m_2 = \frac{1 - v_2^2}{E_2} \quad (13)$$

$$F_{N\text{-unit}} = \frac{F_N}{nb} \quad (14)$$

The equivalent elasticity moduli  $E_1$  and  $E_2$  should be calculated while taking the composite material of the TWUSM into account. The stator consists of piezoelectric ceramic material with a metal medium. The rotor is composed of the contact material and a metal medium. The equivalent elasticity modulus of the composite material can be derived by (15) when two materials are stacked in the thickness direction; their elasticity moduli are  $E_a$  and  $E_b$  with thicknesses of  $t_a$  and  $t_b$ , respectively.

$$E_{tot} = \frac{E_a E_b (t_a + t_b)}{t_a E_b + t_b E_a} \quad (15)$$

The shape coefficient of cylinder  $B$  can be calculated by (16) [15].  $R_l$  can be calculated using the displacement of the stator by (17).  $R_2$  is an infinite value because the rotor is a plate.

$$B = \frac{1}{2} \left( \frac{1}{R_1} + \frac{1}{R_2} \right) \quad (16)$$

$$\frac{1}{R_l} = \frac{\partial^2 w(x)}{\partial x^2} \Big|_{x=0} = \left( \frac{2\pi}{\lambda} \right)^2 \cdot w(x) \Big|_{x=0} = \left( \frac{2\pi}{\lambda} \right)^2 \cdot A \quad (17)$$

### 3.5 Analysis of the normal pressure distribution

Because the normal pressure distribution is proportional to (10), which is the normal displacement of the neutral plane of the stator, the normal pressure distribution  $p(x)$  ( $\text{N/m}^2$ ) on the contacting surface can be derived by (18), where  $X$  ( $\text{N/m}^2$ ) is the amplitude of the normal pressure distribution before the deformation of the stator and where  $C$  is an unknown constant. The unknown constant  $C$  accounts for the boundary conditions, which state that  $p(x)$  should be equal to zero when  $x=-L$  and  $x=L$ . Consequently,  $C$  can be found by (19). The unknown function,  $X$ , can be found using condition (20). Eq. (21) can be induced from the condition under which the normal pressure distribution is symmetric about  $x=0$  and by substituting (18) and (19) into (20). From (21), the amplitude of the normal pressure distribution  $X$  is derived by (22).

$$p(x) = X \left[ \cos\left(\frac{2\pi x}{\lambda}\right) + C \right] \quad (18)$$

$$C = -\cos\left(\frac{2\pi L}{\lambda}\right) \quad (19)$$

$$F_{N\text{-unit}} = \int_{-L}^L p(x) dx \quad (20)$$

$$F_{N\text{-unit}} = 2X \int_0^L \left[ \cos\left(\frac{2\pi x}{\lambda}\right) - \cos\left(\frac{2\pi L}{\lambda}\right) \right] dx \quad (21)$$

$$X = \frac{\pi F_{N\text{-unit}}}{\lambda \left[ \sin\left(\frac{2\pi L}{\lambda}\right) - \frac{2\pi L}{\lambda} \cos\left(\frac{2\pi L}{\lambda}\right) \right]} \quad (22)$$

Finally, the governing equation for the analysis of the normal pressure distribution as a function of the normal force applied to a TWUSM,  $F_N$ , is derived by (23). The maximum pressure  $p_{max}$  can be calculated by  $p(0)$ .

$$p(x) = \frac{\pi F_N \left[ \cos\left(\frac{2\pi x}{\lambda}\right) - \cos\left(\frac{2\pi L}{\lambda}\right) \right]}{nb\lambda \left[ \sin\left(\frac{2\pi L}{\lambda}\right) - \frac{2\pi L}{\lambda} \cos\left(\frac{2\pi L}{\lambda}\right) \right]} \quad (23)$$

### 3.6 Analysis of the stress and the strain

In the case of dynamic contact, the stress can be expressed as normal stress and tangential stress [14, 15]. The normal stress,  $\sigma_{z_n}(x, z)$ , which is induced by normal force can be derived by (24). The tangential stress,  $\sigma_{z_t}(x, z)$ , which is generated by the tangential frictional force can be expressed by (25).

$$\sigma_{z_n}(x, z) = -\frac{z}{\pi} [L\beta(x, z) - x\alpha(x, z)] p_{max} \quad (24)$$

$$\sigma_{z_t}(x, z) = -\frac{1}{\pi} z^2 \alpha(x, z) f_{max}, \quad (25)$$

which are subject to

$$\alpha(x, z) = \frac{\pi}{k_1} \frac{1 - \sqrt{\frac{k_2}{k_1}}}{\sqrt{\frac{k_2}{k_1}} \sqrt{2\sqrt{\frac{k_2}{k_1}} + \left( \frac{k_1 + k_2 - 4L^2}{k_1} \right)}} \quad (26)$$

$$\beta(x, z) = \frac{\pi}{k_1} \frac{1 + \sqrt{\frac{k_2}{k_1}}}{\sqrt{\frac{k_2}{k_1}} \sqrt{2\sqrt{\frac{k_2}{k_1}} + \left( \frac{k_1 + k_2 - 4L^2}{k_1} \right)}} \quad (27)$$

$$k_1 = (L+x)^2 + z^2 \quad (28)$$

$$k_2 = (L-x)^2 + z^2 \quad (29)$$

$$f_{\max} = \mu p_{\max}, \quad (30)$$

where  $\mu$  is the dynamic frictional coefficient.

The stress for the dynamic contact can be expressed by (31). From the Hook's law, Eq. (32) is derived. The strain,  $\varepsilon_z(x, z)$ , can be induced by applying the infinitesimal thickness in the  $z$  direction,  $\Delta t_{stator}$ , as (33).

$$\sigma_z(x, z) = \sigma_{z_n}(x, z) + \sigma_{z_t}(x, z) \quad (31)$$

$$\sigma_z(x, z) = E_z \varepsilon_z(x, z) \quad (32)$$

$$\varepsilon_z(x, z) = \frac{\delta_z(x, z)}{\Delta t_{stator}} \quad (33)$$

Hence, the deformation at a segmented element,  $\delta_z(x, z)$ , can be determined by (34). The total deformation in the  $z$  direction at  $x$  position,  $\delta_{tot\_z}(x)$ , is derived by (35).

$$\delta_z(x, z) = \frac{\sigma_z(x, z)}{E_z} \Delta t_{stator} \quad (34)$$

$$\delta_{tot\_z}(x) = \sum_{z=0}^{t_{tot}} \delta_z(x, z) \quad (35)$$

### 3.7 Analysis of the displacement and the velocity distribution of the stator taking the deformation into consideration

The displacement amplitude of the stator decreased nonlinearly with the deformation caused by the applied normal force and the dynamic contact condition. The deformed normal displacement equation of the stator will be an asymmetric non-linear function due to the dynamic contact condition. Hence, an approximate method is proposed in this research to describe the nonlinear traveling wave of a deformed stator. The normal displacement of the neutral plane of a deformed stator in the plus  $x$  contact area,  $w_{final\_p}(x)$ , and in the minus  $x$  contact area,  $w_{final\_m}(x)$ , in the moving reference can be derived by (36) and (38), respectively. The traveling wave of the neutral plane of a deformed vibrator in the plus  $x$  contact area,  $w_{final\_p}(\hat{x}, t)$ , and in the minus  $x$  contact area,  $w_{final\_m}(\hat{x}, t)$ , in the fixed reference can be induced by (37) and (39), respectively. The total number of unknown constants of (36-39) is eight, in which  $\zeta_p$  and  $\zeta_m$  can be found as the normal displacement when  $x$  equal 0. The remaining six unknown constants can be calculated by solving a  $3 \times 3$  inverse matrix using the three  $x$  position and the associated normal displacement values for each plus and minus contact area.

$$w_{final\_p}(x) = w(x) - \delta_{tot\_z}(x) \quad (36)$$

$$= (\alpha_p x^3 + \beta_p x^2 + \gamma_p x^1 + \zeta_p) \cos(kx)$$

$$w_{final\_p}(\hat{x}, t) = (\alpha_p \hat{x}^3 + \beta_p \hat{x}^2 + \gamma_p \hat{x}^1 + \zeta_p) \cos(k\hat{x} - \omega t) \quad (37)$$

$$w_{final\_m}(x) = w(x) - \delta_{tot\_z}(x) \quad (38)$$

$$= (\alpha_m x^3 + \beta_m x^2 + \gamma_m x^1 + \zeta_m) \cos(kx)$$

$$w_{final\_m}(\hat{x}, t) = (\alpha_m \hat{x}^3 + \beta_m \hat{x}^2 + \gamma_m \hat{x}^1 + \zeta_m) \cos(k\hat{x} - \omega t) \quad (39)$$

The horizontal displacement at the contacting surface of the stator can be derived by applying Kirchhoff's plate theory to (36-39). The horizontal displacement for the plus  $x$  area in the fixed reference,  $u_{x\_p}(\hat{x}, t)$ , can be induced by (40), where  $a$  is the distance from the neutral plane to the contact surface.

$$u_{x\_p}(\hat{x}, t) = -a \frac{dw_{final\_p}(\hat{x}, t)}{dx} \quad (40)$$

$$= -a[(3\alpha_p \hat{x}^2 + 2\beta_p \hat{x} + \gamma_p) \cos(k\hat{x} - \omega t) - k(\alpha_p \hat{x}^3 + \beta_p \hat{x}^2 + \gamma_p \hat{x}^1 + \zeta_p) \sin(k\hat{x} - \omega t)]$$

The horizontal velocity of the stator at the contact surface in the fixed reference,  $v_{s\_p}(\hat{x}, t)$ , can be derived by (41) for the plus  $x$  area.

$$v_{s\_p}(\hat{x}, t) = \frac{du_{x\_p}(\hat{x}, t)}{dt} \quad (41)$$

$$= -a[\omega(3\alpha_p \hat{x}^2 + 2\beta_p \hat{x} + \gamma_p) \sin(k\hat{x} - \omega t) + k\omega(\alpha_p \hat{x}^3 + \beta_p \hat{x}^2 + \gamma_p \hat{x}^1 + \zeta_p) \cos(k\hat{x} - \omega t)]$$

The horizontal velocity of the stator at the contact surface in the moving reference,  $v_{s\_p}(x)$ , can be induced by (42) for the plus  $x$  area by applying (7) and (8) to (41).

$$v_{s\_p}(x) = \frac{du_{x\_p}(x)}{dt} \quad (42)$$

$$= -a[\omega(3\alpha_p x^2 + 2\beta_p x + \gamma_p) \sin(kx) + k\omega(\alpha_p x^3 + \beta_p x^2 + \gamma_p x^1 + \zeta_p) \cos(kx)]$$

The governing equations for the minus  $x$  area can be suggested in the same way as (40-42).

### 3.8 Analysis of the normal pressure distribution considering the deformation of a stator

The normal pressure distribution induced by a nonlinear displacement function which considers the deformation of

the stator at the plus  $x$  contact area of  $p_{final\_p}(x)$  ( $\text{N/m}^2$ ) can be determined by (43), where  $X_{final\_p}$  is the amplitude of the final normal pressure distribution and  $C_{final\_p}$  is an unknown constant at the plus  $x$  contact area. For the minus  $x$  area, the normal pressure displacement can be derived in the same way as (43). The unknown constants can be solved by (44) and (45).

$$\begin{aligned} p_{final\_p}(x) &= X_{final\_p} \left[ w_{final\_p}(x) + C_{final\_p} \right] \\ &= X_{final\_p} \left[ (\alpha_p x^3 + \beta_p x^2 + \gamma_p x^1 + \zeta_p) \cos(kx) + C_{final\_p} \right] \end{aligned} \quad (43)$$

$$\begin{aligned} C_{final\_p} &= -w_{final\_p}(L) \\ &= -(\alpha_p L^3 + \beta_p L^2 + \gamma_p L^1 + \zeta_p) \cos(kL) \end{aligned} \quad (44)$$

$$C_{final\_m} = -w_{final\_m}(-L) \quad (45)$$

The unknown functions  $X_{final\_p}$  and  $X_{final\_m}$  can be induced by conditions (46) and (47).

$$F_{N\_unit\_p} = \int_0^L p_{final\_p}(x) dx \quad (46)$$

$$F_{N\_unit\_m} = \int_{-L}^0 p_{final\_m}(x) dx \quad (47)$$

The normal force per unit length in the radial direction at unit wave,  $F_{N\_unit}$ , is constituted with the force of the plus  $x$  contact area  $F_{N\_unit\_p}$  and that of the minus  $x$  contact area  $F_{N\_unit\_m}$ , as expressed by (48) and (49), respectively.

$$F_{N\_unit\_p} = \frac{\sum_{x=0}^L w_{final\_p}(x)}{\sum_{x=-L}^0 w_{final\_m}(x) + \sum_{x=0}^L w_{final\_p}(x)} \times F_{N\_unit} \quad (48)$$

$$F_{N\_unit\_m} = \frac{\sum_{x=-L}^0 w_{final\_m}(x)}{\sum_{x=-L}^0 w_{final\_m}(x) + \sum_{x=0}^L w_{final\_p}(x)} \times F_{N\_unit} \quad (49)$$

For the plus  $x$  contact area, the unknown function  $X_{final\_p}$  can be determined using (43–49), as follows:

$$\begin{aligned} F_{N\_unit\_p} &= \int_0^L p_{final\_p}(x) dx \\ &= X_{final\_p} \int_0^L \left[ (\alpha_p x^3 + \beta_p x^2 + \gamma_p x^1 + \zeta_p) \cos(kx) + C_{final\_p} \right] dx \quad (50) \\ &= X_{final\_p} [F_{int}]_0^L \end{aligned}$$

Eq. (50) can be modified to (51). For the minus contact

area, (52) can be derived from (50).

$$X_{final\_p} = \frac{F_{N\_unit\_p}}{[F_{int}]_0^L} \quad (51)$$

$$X_{final\_m} = \frac{F_{N\_unit\_m}}{[F_{int}]_{-L}^0}, \quad (52)$$

where the integration part can be expressed by:

$$\begin{aligned} [F_{int}]_i^j &= [\{\alpha_p k^3 x^3 \sin(kx) + 3\alpha_p k^2 x^2 \cos(kx) \\ &\quad - 6\alpha_p \cos(kx) - 6\alpha_p kx \sin(kx) \\ &\quad + \beta_p k^3 x^2 \sin(kx) + 2\beta_p k^2 x \cos(kx) \\ &\quad - 2\beta_p k \sin(kx) + \gamma_p k^3 x \sin(kx) + \gamma_p k^2 \cos(kx) \\ &\quad + \zeta_p k^3 \sin(kx) + C_{final\_p} k^4 x\} / k^4]_i^j \end{aligned} \quad (53)$$

Finally, the normal pressure distribution taking into account the nonlinearly deformed stator is proposed in this research as (54) and (55).

$$p_{final\_p}(x) = \frac{F_{N\_unit\_p}}{[F_{int}]_0^L} [w_{final\_p}(x) - w_{final\_p}(L)] \quad (54)$$

$$p_{final\_m}(x) = \frac{F_{N\_unit\_m}}{[F_{int}]_{-L}^0} [w_{final\_m}(x) - w_{final\_m}(-L)] \quad (55)$$

### 3.9 Analysis of the motor performance

The horizontal velocity distribution of a deformed stator considering dynamic contact has an asymmetric shape, as shown in Fig. 4. Hence, the slip distribution between the rotor and the stator can be described by Fig. 5.

From Fig. 6, the frictional force acting on the surface of the stator at unit wave,  $F_{fric}$  ( $\text{N/m}$ ), can be induced by (56), where  $N$  (rpm) denotes the revolutions per minute of the rotor.

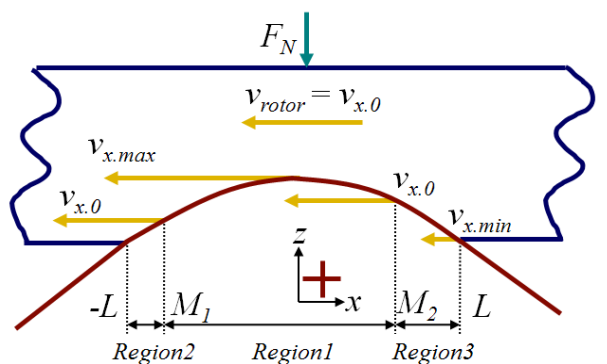


**Fig. 4.** Distribution of the horizontal velocity at the stator and the rotor considering the nonlinear deformation induced by dynamic contact.

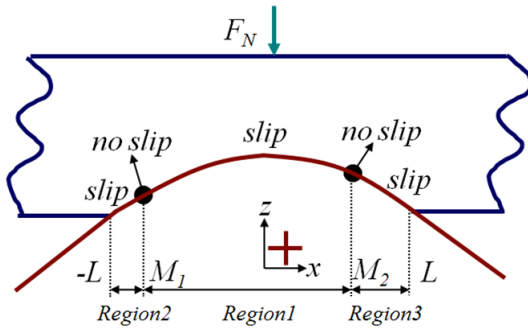


**Fig. 5.** Slip distribution over the nonlinearly deformed contact area caused by dynamic contact.

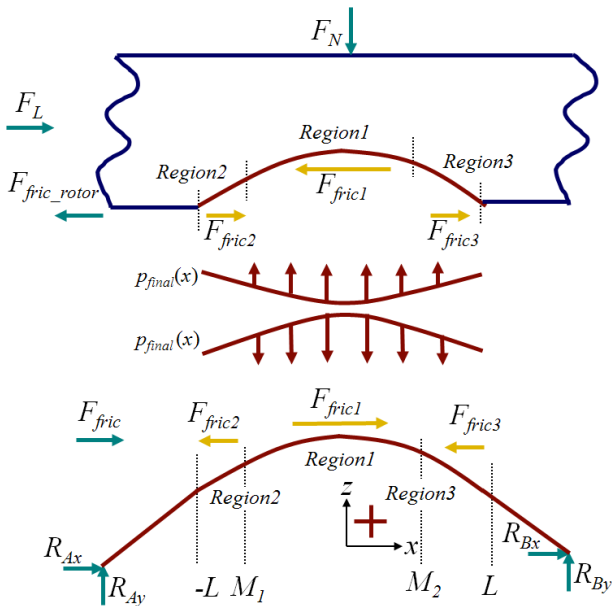


**Fig. 6.** Free-body diagram to elucidate the forces acting on the rotor and the stator.

$$F_{flic} = -\mu \int_{-L}^L \text{sign} \left[ v_s(x) - \frac{2\pi N}{60} r_{eff} \right] p_{final}(x) dx \quad (56)$$

when  $(0 \leq x \leq L)$ ,

$$v_s(x) = v_{s\_p}(x), \quad p_{final}(x) = p_{final\_p}(x) \quad (57)$$

when  $(-L \leq x \leq 0)$ ,

$$v_s(x) = v_{s\_m}(x), \quad p_{final}(x) = p_{final\_m}(x) \quad (58)$$

which is subject to,

$$\text{sign} [\tau] = 1, \text{ if } \tau > 0$$

$$\text{sign} [\tau] = 0, \text{ if } \tau = 0$$

$$\text{sign} [\tau] = 1, \text{ if } \tau < 0$$

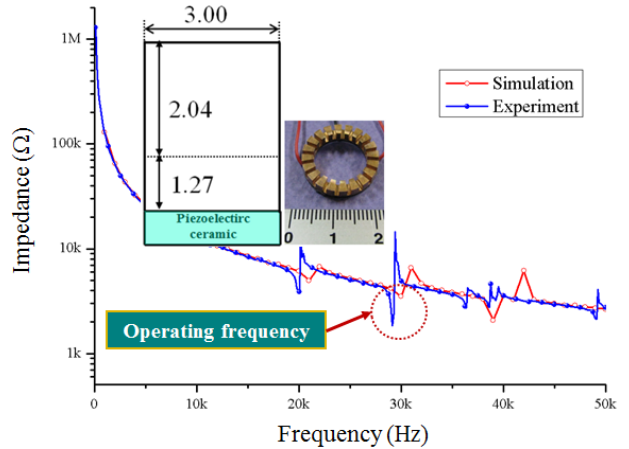


**Fig. 7.** Shape of prototype and its impedance.

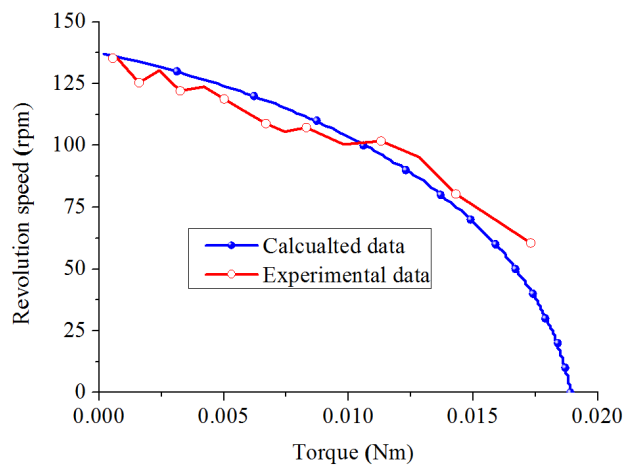


**Fig. 8.** Speed-torque curve of TWUSM.

The total frictional force acting on the surface of the stator,  $F_{flic\_tot}$  (N), can be derived by (59), which is subject to (57) and (58).

$$F_{flic\_tot} = -\mu nb \int_{-L}^L \text{sign} \left[ v_s(x) - \frac{2\pi N}{60} r_{eff} \right] p_{final}(x) dx \quad (59)$$

The total load force acting on the rotor,  $F_{L\_tot}$  (N) can be expressed by  $nbF_L$ . It has the same meaning as the total friction force of the rotor,  $F_{flic\_rotor\_tot}$  (N), as induced by (60), which also can be used for the calculation of the thrust force of the linear TWUSM.

$$\begin{aligned} F_{L\_tot} &= F_{flic\_rotor\_tot} = -F_{flic\_tot} \\ &= -nb(F_{flic1} - F_{flic2} - F_{flic3}) \end{aligned} \quad (60)$$

The torque  $M_f$  (Nm) and the speed  $N$  (rpm) of the ring-type TWUSM can be analyzed by (61), which is subject to (57) and (58).

$$M_f = r_{eff} F_{L\_tot} = -r_{eff} F_{fric\_tot}$$

$$= r_{eff} \mu n b \int_{-L}^L \text{sign} \left[ v_s(x) - \frac{2\pi N}{60} r_{eff} \right] p_{final}(x) dx \quad (61)$$

#### 4. Verification of Analysis Method

As shown in Fig. 7, the stator is prototyped and its impedance is measured and calculated. As displayed in Fig. 7, the calculated data are in good agreement with the experimental results. Hence, it is verified that the 3D-FEM used in this research is correct.

The speed-torque is analyzed using the proposed characteristic analysis method derived from CDCM. These results are then compared to the experimental data, as illustrated in Fig. 8. The analysis results are fitted well with the experimental data. These results prove that the proposed characteristic analysis method is correct. It takes about 1-2 seconds for the analysis using the proposed characteristic analysis method. Hence, the usefulness of the proposed analysis method is validated. As displayed in Fig. 9, the stress distribution at the contact area of the stator shows an asymmetric and nonlinear shape due to the consideration of dynamic contact. The material coefficients used for the characteristic analysis are included in APPENDIX and are shown in Table 1.

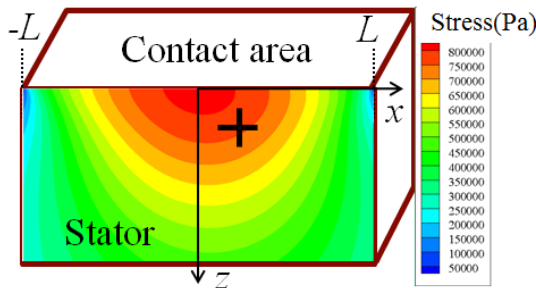


**Fig. 9.** Calculated stress distribution at the stator using the CDCM.

**Table 1.** Parameters for the analysis of the TWUSM

| Parameter   | Symbol  | Value     |
|---|---------|-----------|
| Applied normal force                                  | $F_N$   | 15(N)     |
| Number of wave cycles                                 | $n$     | 5         |
| Outer diameter of the TWUSM                           |         | 0.02(m)   |
| Inner diameter of the TWUSM                           |         | 0.14(m)   |
| Elasticity modulus for the aluminum of the rotor      | $E_a$   | 70.0(GPa) |
| Elasticity modulus for the contact layer of the rotor | $E_b$   | 0.58(GPa) |
| Poisson's ratio of the stator                         | $\nu_1$ | 0.35      |
| Poisson's ratio of the rotor                          | $\nu_2$ | 0.35      |
| Dynamic frictional coefficient                        |         | 0.15      |

#### 5. Conclusion

The contact mechanism of the TWUSM is a complex nonlinear problem, which makes it difficult to propose a useful contact model and a feasible motor performance analysis method. Hence, it is noteworthy from the fact that a correct and useful characteristic analysis method using CDCM is proposed in this research.

#### Appendix

##### (1) PZT (z-axis poling):

Mechanical stiffness matrix for the constant electric field  $E$ ;  $c^E$  (N/m<sup>2</sup>)

$$= \begin{bmatrix} 13.25 & 6.94 & 6.46 & 0.0 & 0.0 & 0.0 \\ 6.94 & 13.25 & 6.46 & 0.0 & 0.0 & 0.0 \\ 6.46 & 6.46 & 10.52 & 0.0 & 0.0 & 0.0 \\ 0.0 & 0.0 & 0.0 & 2.68 & 0.0 & 0.0 \\ 0.0 & 0.0 & 0.0 & 0.0 & 2.68 & 0.0 \\ 0.0 & 0.0 & 0.0 & 0.0 & 0.0 & 3.16 \end{bmatrix} 10^{10}$$

Piezoelectric coefficient;  $e$  (C/m<sup>2</sup>)

$$= \begin{bmatrix} 0.0 & 0.0 & 0.0 & 0.0 & 12.82 & 0.0 \\ 0.0 & 0.0 & 0.0 & 12.82 & 0.0 & 0.0 \\ -6.61 & -6.61 & 13.5 & 0.0 & 0.0 & 0.0 \end{bmatrix}$$

Permittivity for the constant mechanical strain  $S$ ;  $s$  (F/m<sup>2</sup>)

$$= \begin{bmatrix} 7.32 & 0.0 & 0.0 \\ 0.0 & 7.32 & 0.0 \\ 0.0 & 0.0 & 6.28 \end{bmatrix} 10^{-9}$$

Density;  $\rho$  (kg/m<sup>3</sup>) = 7500

Mechanical quality factor;  $Q$  = 900

##### (2) Elastic body of the stator (Phosphor-bronze):

Mechanical stiffness matrix;  $c_m$  (N/m<sup>2</sup>)

$$= \begin{bmatrix} 179.75 & 96.79 & 96.79 & 0.0 & 0.0 & 0.0 \\ 96.79 & 179.75 & 96.79 & 0.0 & 0.0 & 0.0 \\ 96.79 & 96.79 & 179.75 & 0.0 & 0.0 & 0.0 \\ 0.0 & 0.0 & 0.0 & 41.481 & 0.0 & 0.0 \\ 0.0 & 0.0 & 0.0 & 0.0 & 41.481 & 0.0 \\ 0.0 & 0.0 & 0.0 & 0.0 & 0.0 & 41.481 \end{bmatrix} 10^9$$

Density;  $\rho_m$  (kg/m<sup>3</sup>) = 8780

Mechanical quality factor;  $Q_m$  = 3000

## References

- [1] J. Wallaschek, "Contact mechanics of piezoelectric ultrasonic motors," *Smart Materials and Structures*, Vol. 7, No. 3, pp. 369-381, Jun. 1998.
- [2] H. Stork and J. Wallaschek, "The effect of tangential elasticity of the contact layer between stator and rotor in traveling wave ultrasonic motors," *International journal of Non-Linear Mechanics*, Vol. 38, pp. 143-159, 2003.
- [3] J.-T. Zhang, H. Zhu, S.-Q. Zhou, Chun-Sheng Zhao, "Optimal design of a rod shape ultrasonic motor using sequential quadratic programming and finite element method," *Sensors and Actuators*, Vol.59, pp.11-17, Oct. 2012.
- [4] K.-J. Lim, S.-H. Park, Y.-J. Yun, K.-Y. Lee, S.-H. Kang, J.-S. Lee and S.-H. Jeong, "Characteristics of Disk-type Linear Ultrasonic Motor for Application to x-y Stage," *Journal of Electrical Engineering & Technology*, Vol. 1, No. 1, pp.101-105, 2006.
- [5] S.B Choi and D.H Lee, "Modal analysis and control of a bowl parts feeder activated by piezoceramic actuators," *Journal of Sound and Vibration*, Vol.275, Issue 1-2, pp.452-458, Aug. 2004.
- [6] J.-S. Rho, C.-H. Lee, H.-K. Jung, "Optimal design of ultrasonic motor using evolution strategy and finite element method," *International Journal of Applied Electromagnetics and Mechanics*, Vol. 25, No. 1-4, Jul. 2007.
- [7] H. H and Ueha S, "Revolution speed characteristics of an ultrasonic motor estimated from the pressure distribution of the rotor," *Proc. 12th Symp. on Ultrasonic Electronics*, Tokyo, Japan, 1991.
- [8] T. Maeno and D. B. Bogy, "Effect of the hydrodynamic bearing on rotor/stator contact in a ring-type ultrasonic motor," *IEEE Transactions on Ultrasonics, Ferroelectrics, and Frequency Control*, Vol. 39, pp. 675-82, 1992.
- [9] H. Hirata and S. Ueha, "Design of a Traveling Wave Type Ultrasonic Motor," *IEEE Transactions on Ultrasonics, Ferroelectrics, and Frequency Control*, Vol. 42, No. 2, Jul. 1995.
- [10] A. M. Flynn, "Piezoelectric ultrasonic micromotors," *PhD Thesis*, Department of Electrical Engineering and Computer Science, Massachusetts Institute of Technology, 1995.
- [11] X. Cao, J. Wallaschek, "Estimation of the tangential stresses in the stator/rotor of traveling wave ultrasonic motors using visco-elastic foundation model," *Proceedings of 2nd Int. Conference on Contact Mechanics*, Vol. 2, pp. 53-61, 1995.
- [12] J. P. Schmidt, P. Hagedorn, and M. Bingqi, "A note on the contact problem in an ultrasonic travelling wave motor," *Int. J. Nonlinear Mech.*, Vol. 31, pp. 915-924, 1996.
- [13] J. Qu, F. Sun, C. Zhao, "Performance evaluation of traveling wave ultrasonic motor based on a model with visco-elastic friction layer on stator," *Ultrasonics*, Vol. 45, pp. 22-31, 2006.
- [14] J. O. Smith and C. K. Lui, "Stresses due to tangential and normal loads on an elastic solid with application to some contact stress problems," *J. App. Mech. Trans. ASME*, Vol.75, pp. 157-166, 1953.
- [15] R. L. Norton, *MACHINE DESIGN: An Integrated Approach*, Third Edition, Pearson Prentice Hall, Pearson Education. Inc., Chapter 6., 2006.



**Jong-Suk Ro** He received the B.S. degree in Mechanical Engineering from Han-Yang University, Seoul, Korea, in 2001. In 2008, he earned a PhD in Electrical engineering from Seoul National University, Seoul, Korea, through the Combined Master's and Doctorate Program. He conducted

research on cellular phone modules at R&D center of Samsung Electronics as a Senior Engineer from 2008 to 2012. From 2012 to 2013, he was at Brain Korea 21 Information Technology of Seoul National University as a Post-Doctoral Fellow. Currently, he is carrying out research at Electrical Energy Conversion System Research Division of Smart Grid Team at Korea Electrical Engineering & Science Research Institute as a Researcher. His research interests are interdisciplinary research, energy conversion device, camera module, numerical analysis, and optimal design of electric machines.



**Kyung-Pyo Yi** He received the B.S. and M.S. degree from the School of Electrical and Electronics Engineering, Seoul National University, Seoul, Korea in 2007 and 2009, respectively. He is currently a Ph.D. student at Seoul National University, Seoul, Korea. His research focuses on analysis and design of piezoelectric devices, electric motors and superconducting magnetic energy storage(SMES).



**Tae-Kyung Chung** He received the B.S., M.S., and Ph.D. degrees in electrical engineering from Seoul National University in 1981, 1983, and 1987, respectively. From 1986 to 1987, he worked at Daewoo Heavy Industries as a senior researcher. Since 1988, he has been with the School of Electrical and Electronics Engineering at Chung Ang University in Korea as a professor. In 1991, he was with Harvey Mudd College in California as a visiting scholar. His main research fields are design of electric motors and actuators.



**Hyun-Kyo Jung** He received the B.S., M.S., and Ph.D. degree in Electrical engineering from the Seoul National University, Seoul, Korea, in 1979, 1981, and 1984, respectively. From 1985 to 1994, he was a member of the faculty with Kangwon National University. From 1987 to 1989, he was with the Polytechnic University of Brooklyn, Brooklyn, NY. From 1999 to 2000, he was a Visiting Professor with the University of California at Berkeley. He is currently a Professor at the School of Electrical Engineering and Computer Science/Electrical Engineering, Seoul National University. His research interests are the analysis and design of the electric machine.